Effects of Mass Flow Rate Imbalance Among Petals During T_{CS} Measurements of ITER TF Short Samples in SULTAN

L. Savoldi Richard, F. Bellina, M. Breschi, P. L. Ribani, F. Subba, and R. Zanino

***Abstract*—Since year 2009, the joint of the toroidal field (TF) conductor samples tested in the SULTAN facility at PSI Villigen, CH, is solder-filled, so that the helium coolant can only flow axially inside the central channel. The latter is however plugged starting ~40–45 mm downstream of the joint. The helium has then to pass from the central channel into the annular cable region over such a short length that the desired homogeneity of the flow distribution among the petals in the high field region is not guaranteed a priori, since central helix and petal wrappings act as azimuthally non-uniform obstacles to the radial flow. In the paper we first present a geometrical model for estimating this interference to the radial flow, and combine it with a CFD (ANSYS-FLUENT) model of the hydraulic effect of the plug, in order to estimate the mass flow rate imbalance among the petals at the beginning of the plug. This is then used as boundary condition by the THELMA code, to parametrically assess the results of a T_{CS} measurement.**

***Index Terms*—Fusion reactors, simulation, superconducting coils.**

I. Introduction

In the frame of the International Thermonuclear Experimental Reactor (ITER) qualification program, several short toroidal field (TF) conductor samples are being tested for DC characterization in the SULTAN facility at PSI Villigen, CH [1].

The geometry of either leg of the SULTAN sample is sketched in Fig. 1, where the originally vertical sample with forced supercritical helium (SHe) flow from bottom to top is represented horizontally with flow from the left to the right. We see that there are basically four regions for the flow: 1) the soldered joint where He flows only in the central channel; 2) the region just downstream of the joint where He can flow radially to the annular cable region, impeded only by the central channel spiral; 3) the next region downstream, up to the beginning of the plug, where however radial flow is impeded also by the petal wrappings; 4) the region of the plug, including the high field region, where He can flow only in the cable annulus.

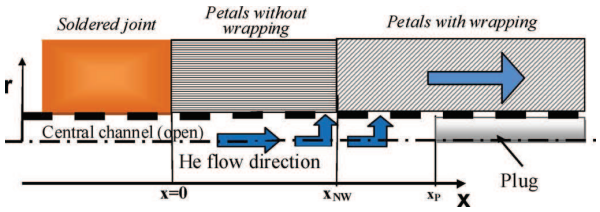

Fig. 1. Sketch of conductor geometry in the joint-to-plug region. The origin of the x coordinate is set at the joint outlet; x_{NW} is where the petal wrapping starts, x_P where the plug starts.

Helium can enter one of the petals only at those locations where the contact surface between the cable region and the central channel is not obstructed by the central channel spiral, or by the petal wrapping. These locations depend on the spiral and wrapping pitches and perforations and, since $x_P \ll L_P$ (the petal pitch ~450 mm), the open area allowing communication between cable region and central channel will vary from petal to petal, favoring a non-uniform flow distribution.

In addition, even if the open areas between the central channel and the petals were equally distributed, this would not necessarily guarantee a uniform distribution among the petals of the axial mass flow rate. In fact, such uniformity would require the radial He flux through an elemental open area dA_i between central channel and i-th petal to be independent of the location of the area dA_i. However, since the driver which forces He to move from the central channel to the petals region is the pressure difference between the two regions, and the pressure profile along the channel is strongly influenced by the presence of the final plug, we can expect that the radial flux will increase as distance of dA_i from the plug decreases.

Here we model this complex situation as follows: a) compute, by a purely geometrical 3-D model, the fraction of total open area for radial He flow to the i-th petal; b) compute, using the commercial CFD code ANSYS-FLUENT, the longitudinal distribution of the radial mass flux to the i-th petal induced by the plug. The two effects are then combined to obtain an estimate of the distribution of the mass flow rate among the different petals at the beginning of the plug.

Manuscript received August 03, 2010; accepted October 03, 2010. This work was supported in part under Contract ITER/CT/08/1286 to University of Bologna and Contract CTR. 407/2010 between University of Bologna and Dipartimento di Energetica, Politecnico di Torino.

L. Savoldi Richard, F. Subba, and R. Zanino are with Dipartimento di Energetica, Politecnico di Torino, 10129 Turin, Italy (e-mail: laura.savoldi@polito.it).

F. Bellina is with University of Udine, Udine - 0432 558111, Italy.

M. Breschi and P. L. Ribani are with University of Bologna, 40126 Bologna, Italy.

Color versions of one or more of the figures in this paper are available online at http://ieeexplore.ieee.org.

Digital Object Identifier 10.1109/TASC.2010.2087732

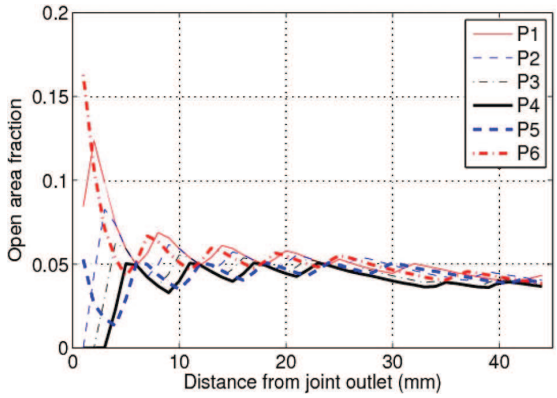

Fig. 2. Distribution along the conductor of the open area fraction for each petal for a typical set of geometrical parameters.

II. Analysis of He Flow Inhomogeneity Among Petals

A. Geometrical Model for the Open Area Fraction

We introduce the function $\chi_{\rm i}({\rm x},\vartheta)$: $\chi_{\rm i}=1$ if at the corresponding location $({\rm x},\vartheta)$, where ϑ is the azimuthal coordinate, the interface between the central channel and the i-th petal is open; otherwise $\chi_{\rm i}=0$. $\chi_{\rm i}$ can be easily computed for any given set of geometrical parameters (see Section II-C). The resulting distributions of the open area fraction (with respect to the total open area) $g_{\rm i}({\rm x})=\int\chi_{\rm i}({\rm x},\vartheta){\rm d}\vartheta/\Sigma_{\rm i}\int\chi_{\rm i}({\rm x},\vartheta){\rm d}\vartheta$, along the CICC and for each petal, are reported in Fig. 2, showing that 10–20 mm are needed to reach uniformity among the petals (i.e. $g_i\sim 1/6$).

B. CFD Model for the Plug Effect

The plug is the main driver for SHe transport from the central channel to the cable region, because of the resulting pressurization. In other words, because of the much lower hydraulic impedance the He will try to flow as long as possible in the central channel and move to the cable only when this cannot be avoided.

To model this effect we introduce a 2D, 2-region steady state model of the CICC, as already presented in [2]. The two coordinates represent the axial (x) and the radial (r) directions. The domain is composed by two regions: the central channel, with turbulent He flow, delimited by a finite thickness spiral, and the cable region, treated like a porous medium, introducing a Darcy-Forchheimer constitutive relation for the friction in the momentum conservation equation, with coefficients determined as described in [2] and references therein. At the walls of the porous region, the standard no-slip condition is enforced, while at the outflow boundary zero normal gradient is enforced to guarantee a smooth behavior of the solution. The petals are not distinguished by the model, as its main purpose is to determine the axial distribution of the radial flow transferred between the central channel and the cable region. As opposed to [2], the wrappings are taken into account by reducing the effective perforation of the spiral for ${\rm x_W}<{\rm x}<{\rm x_P}$. In Fig. 3 we see a typical set of streamlines computed by the code.

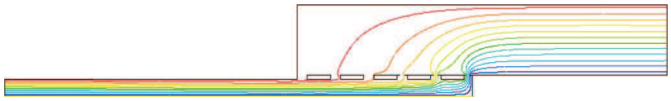

Fig. 3. Streamlines in the central channel and cable regions computed by FLUENT.

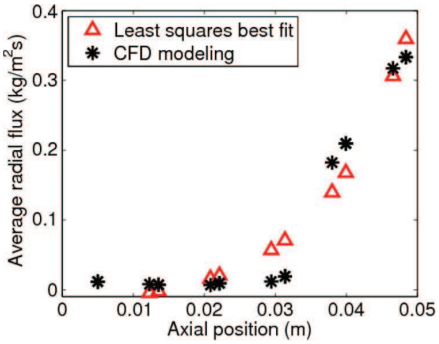

Fig. 4. Axial distribution of the radial flux $\langle{\rm F}\rangle$ from the central channel to the cable bundle computed by FLUENT.

The axial distribution of the He radial flux is computed by the code as follows: for every open segment (x_{start},x_{end}) of the interface between central channel and cable region, we evaluated the average He flux as in (1):

$$\langle F\rangle=\frac{1}{x_{end}-x_{start}}\int_{x_{start}}^{x_{end}}F(x,r_{\rm int})dx \tag{1}$$

The results are shown in Fig. 4. In order to account for different possible (axial) placements of the channel helix with respect to the plug, we have also considered two limiting spiral geometries, shifted one with respect to the other. The results presented here refer to an axisymmetric model. (A similar computation was produced also for a slab (Cartesian) geometry, which gave a qualitatively similar solution.) It is seen that the shape of $\langle F\rangle(x)$ does not depend, in a first approximation, on the exact distribution of the open segments. $F(x)$ can be approximated by (2):

$$F(x,r_{\rm int})=\chi(x)(a+be^{x/L}) \tag{2}$$

where the parameters a, b and L have been evaluated by a least-square fit. In the following we shall assume that the parameter L ($\sim$0.012 m) depends mostly on the plug position, and only very weakly on other details like the exact helix/wrapping position, perforated fraction and pitch. With this assumption, we can proceed to evaluate the He mass flow distribution among the petals in a number of different 3D configurations.

C. Estimate of Flow Inhomogeneity Among Petals

We consider now the real 3D geometry. The helium entering the i-th petal W_i (kg/s) is given by (3):

$$W_i=\int_0^{2\pi}r_{\rm int}d\vartheta\int_0^{x_P}F_i(x,\vartheta,r_{\rm int})dx. \tag{3}$$

and, based on the results above, we can assume

$$F_i(x, \vartheta, r_{\rm int}) = k\chi_i(x, \vartheta)(a + be^{x/L}) \tag{4}$$

where the normalization constant k is introduced in order to allow preserving the total flux. It is then easy to compute the fraction $f_{\rm i}$ of He flowing in the *i-th* petal at the beginning of the plug as in (5):

$$f_i = \frac{W_i}{\Sigma_i W_i} \tag{5}$$

where the integrals defining the W_i are computed with a Monte-Carlo algorithm.

In order to obtain a conservative estimate of the flow inhomogeneity among petals we selected a number of cases, covering the space of the free parameters in the conductor geometry setup. The parameters for the scan and the corresponding ranges consist of: wrapping width (reference 13.5 mm, range (12–15)), petal pitch length (reference 450 mm, range (410–490)), cable initial phase (reference 0°, range ±30°), wrapping initial phase (chosen at random). The $f_{\rm i}$ distribution with the biggest spread among those considered in our parametric study has a minimum of 10.9% and a maximum of 22.5%. This most conservative distribution will be used as boundary condition in what follows.

III. THELMA Code Analysis of an ITER TF Sample Tcs Test in SULTAN

The so-called USTF4 sample [3] is an ITER TF sample which was tested in 2009. In the case of, e.g., the left leg, standard instrumentation includes: voltage crowns VH1 and VH3, with six voltage taps each, located 225 mm upstream and downstream, respectively, of the center of the high-field zone (HFZ); temperature rings T1 and T3, with four thermometers each, located 400 mm upstream and downstream, respectively, of the center of the HFZ. These sensors are utilized to measure T_{CS} by means of two standardized procedures for the voltmetric and calorimetric assessment [4], [5]. No petal-level diagnostics is available for the mass flow rate distribution (the other major ingredient of calorimetry), and we have to rely on codes for that, as well as for the translation of the information measured on the jacket into corresponding knowledge inside the cable.

In view of the above, we try and use here the THELMA code [6] in two steps: in the first one, which we may call of qualitative validation, we shall consider as reference run # USTF4D260501, a $\rm T_{CS}$ test @ $\rm B_{SULTAN} \sim 10.78$ T performed after 600 cycles, and verify to what extent the code is able to reproduce the main measured features of the test, with particular reference to temperature gradients; after that, we shall use the code as a simulator of a typical $\rm T_{CS}$ test, following a suitably extended protocol to allow the inclusion of mass flow rate inhomogeneities on the cross section, in order to estimate how these can affect the interpretation of the test and the major outcome of the measurement.

A. Analysis of Run # USTF4D260501

In this test, the current I is first ramped up in steps to 68 kA, the nominal ITER TF *coil* operating current, then the He inlet temperature $\rm T_{in}$ to the sample is ramped up in steps using a resistive heater until quench. The two quantities $I(\rm t)$ and $T_{in}(\rm t)$ are imposed as external drivers of the transient in the electromagnetic (EM) and thermal-hydraulic (TH) modules of the code, respectively.

We simulate the portion of conductor between lower joint and upper termination *both excluded*, discretizing the CICC in macro-regions as follows:

- For the EM module
  1) 6 cable elements (CE)+12 *straight* jacket elements (JE), or alternatively, in order to verify the numerical convergence/independence of discretization, 36 CE + 36 *straight* JE
- For the TH module
  1) 6 *twisted* [(CE + He channel) = petal + JE], or alternatively, in order to verify the numerical convergence/independence of discretization, 6 *twisted* [(**6** CE + He channel) = petal + JE]
  2) Central channel plugged
     The electrical (in particular lower joint and termination) parameters needed in the EM module are obtained by modeling the solder filled joint through a lumped parameter circuit [7], and then deriving equivalent n-pole matrices.

In the TH module the following boundary conditions are imposed:

- $\rm p_{in}$, $\rm p_{out}$ and $\rm T_{in}$ (where the latter already accounts for the Joule heat generated in lower joint)
- Mass flow redistribution between neighboring petals, driven by local (radial) $\Delta \rm p$
- In two petals, modified friction factor to conservatively impose the most imbalanced mass flow rate distribution corresponding to the results of Section II above.

If we compare simulations and experiment we notice first of all (not shown) that the measured voltages on the given cross section show a significantly larger spread (± 10 μV) than the computed ones (± 2 μV), while the average voltages are in reasonably good agreement.

If we consider the temperature, and in particular the temperature gradients on the cross section just downstream of the HFZ, the result of the simulation strongly depends on the mass flow rate distribution among petals assumed as boundary condition, while the global (averaged) temperature evolution is only marginally affected. If we apply a uniform distribution of the mass flow rate among the petals at the conductor inlet (just downstream of the lower joint), then we see in Fig. 5 that the computed helium temperature gradients on the cross section essentially vanish for most of the transient. If, on the other hand, we consider as boundary condition the distribution computed in Section II, we see in Fig. 5 that the agreement between simulation and experiment is both qualitatively and quantitatively rather good, clearly emphasizing the role of the mass flow rate nonuniformity to explain this feature of the experimental results.

In Fig. 5 we may clearly identify three phases:

- The current steps, during which temperature gradients develop which are however related to the magneto-resistance (as confirmed by the fact that in the baseline runs @ $\rm B_{SULTAN} \sim 0$ T these gradients are not present) and, as such, treated as offset here [8]

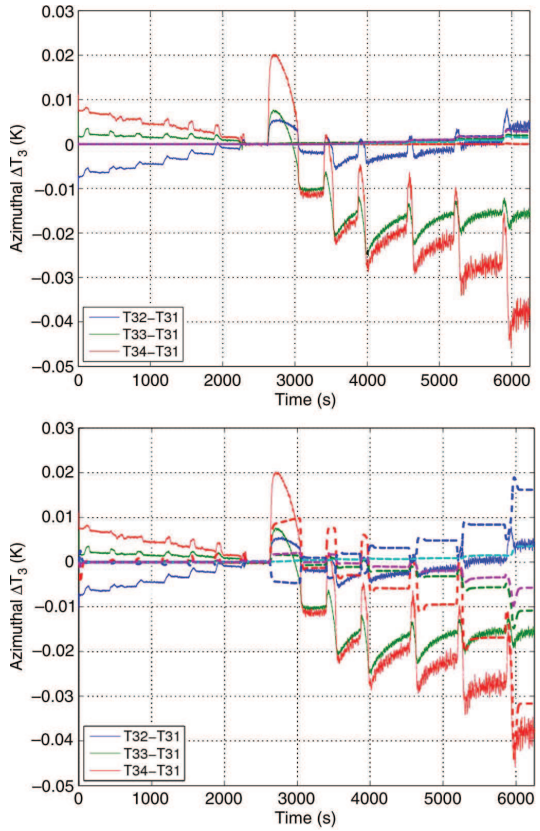

Fig. 5. Comparison between computed (dashed) and measured (solid) temperature gradients on the sample cross section just downstream of the HFZ: Top—uniform inlet mass flow rate distribution among petals, Bottom—imbalanced inlet mass flow rate distribution among petals from Section II.

- An intermediate phase, at the beginning of the T_{in} staircase, characterized by "bumps" in the temperature gradients, due to different He speed transporting the steps of T_{in} in different petals, see Fig. 6, followed by incomplete recovery of the conditions before the bump, due to the increasingly different heights of the steps in different petals, because of the effect of Joule heating on different petals, characterized by different mass flow rates
- A final phase, leading to the quench, where nonlinear amplification of the temperature gradients on the cross section occurs (in the petal with the smallest mass flow rate, Joule heating causes the highest temperature increase, further choking the flow).

B. Interpretation of T_{CS} Measurements

According to the standard protocol, which assumes uniform mass flow rate distribution among the petals, the estimated value for the T_{CS} in the run analyzed above is ~6.6 K. We have generalized that protocol to include the possibility of different mass flow rates (and different temperatures) in the different petals. However, it turns out that the value of T_{CS} is almost unchanged, with differences of the order of 0.01 K. This is clearly understandable if we observe that in run # USTF4D260501 T_{CS} is

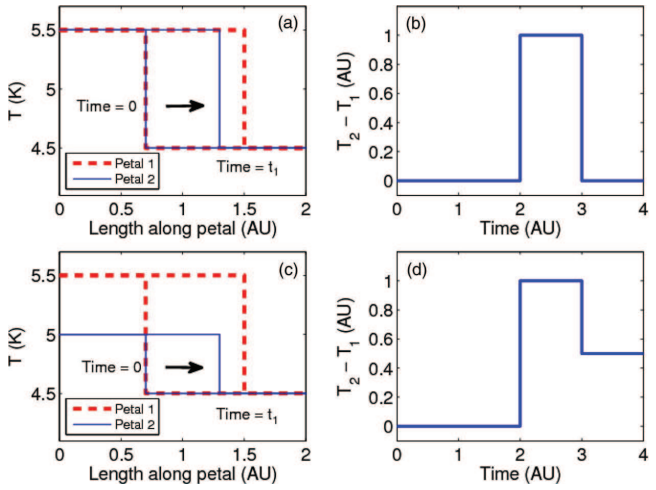

Fig. 6. Ideal spatial propagation of temperature steps of the same height (a) and of different heights (c) in adjacent petals, as due to pure advection with different speeds. Subsequent temperature difference evolution in time (b and d, respectively).

reached at $t \sim 4000$ s, i.e., at a time when the spread of temperatures on the CICC cross section is still rather small (see Fig. 5).

IV. Conclusion

Azimuthal temperature gradients arising during T_{CS} tests of ITER TF samples in SULTAN have been related to mass flow rate inhomogeneities among the petals by self-consistent thermal-hydraulic electromagnetic analysis using the THELMA code. In turn, these mass flow rate inhomogenities have been quantitatively explained as caused by the combined effect of obstructions to the radial flux from the central channel to the cable bundle and of the plug blocking the central channel downstream of the joint. Notwithstanding these inhomogeneities on the conductor cross section, the calorimetric assessment of the T_{CS} appears to be only marginally affected.

References

[1] P. Bruzzone, B. Stepanov, and R. Wesche, "Qualification tests for ITER TF conductors in SULTAN," *Fus. Eng. Des.*, vol. 84, pp. 205–209, 2009.
[2] R. Zanino, S. Giors, and L. Savoldi Richard, "CFD model of ITER CICC. Part VI: Heat and mass transfer between cable region and central channel," *Cryogenics*, vol. 50, pp. 158–166, 2010.
[3] B. Stepanov, P. Bruzzone, R. Wesche, N. Martovetsky, D. Hatfield, A. Vostner, and A. Devred, "Impact of sample preparation procedure on the test results of four US ITER TF conductors," *IEEE Trans. Appl. Supercond.*, vol. 20, pp. 508–511, 2010.
[4] D. Bessette, M. Breschi, C. Calzolaio, A. Devred, M. Menarini, and K. Seo, "Sensitivity analysis of Tcs measurement on ITER TF conductors," *IEEE Trans. Appl. Supercond.*, vol. 20, pp. 1488–1491, 2010.
[5] L. Savoldi Richard and R. Zanino, "Application of calorimetry to the assessment of ITER Nb3Sn TF conductor sample performance in SULTAN tests," *Supercond. Sci. Technol.*, vol. 21, p. 105004, 2008.
[6] M. Ciotti, A. Nijhuis, P. L. Ribani, L. Savoldi Richard, and R. Zanino, "THELMA code electromagnetic model of ITER superconducting cables and application to the ENEA stability experiment," *Supercond. Sci. Technol.*, vol. 19, pp. 987–997, 2006.
[7] F. Bellina, M. Breschi, and P. L. Ribani, "Analysis of the ITER SULTAN sample test conditions with different joint technologies," *IEEE Trasn. Appl. Supercond.*, vol. 20, pp. 482–496, 2010.
[8] M. Bagnasco, "Calorimetric method for current sharing temperature measurements in ITER conductor samples in SULTAN," *Fus. Eng. Des.*, vol. 84, pp. 423–426, 2009.